Comparative Study of Linear and Nonlinear Passivity-Based Control Methods for Switched-Mode Power Supplies in Audio Amplification Systems

T. R. Oliveira
Instituto Federal de Minas Gerais - IFMG
Automation - Campus Betim
Betim, MG - BRAZIL
E-mail: thiago.oliveira@ifmg.edu.br

P. F. Donoso-Garcia, S. I. Seleme Jr., L. M. F. Morais
Universidade Federal de Minas Gerais - UFMG
Department of Electronic Engineering
Belo Horizonte, MG - BRAZIL
E-mails: pedro@cpdee.ufmg.br, seleme@cpdee.ufmg.br, lenin@cpdee.ufmg.br

***Abstract*—This paper presents the comparison of linear and nonlinear passivity-based controllers used to enhance the performance of power supplies employed in audio amplification systems. Theoretical analysis and experimental results have shown that passivity-based control topologies can reduce the output impedance of the power supply, thus providing low level ripple on the voltage rails and allowing the reduction of the power supply output capacitor.**

I. Introduction

The power supply unit employed in audio amplification systems should provide high levels of load and line regulations and maintain low ripple amplitude on the voltage rails, in order to not interfere with the amplifier output signal and thus guarantee high audio quality [1]. All these requirements could not be fulfilled with conventional unregulated topologies, which are still the major structure used in amplification systems. Even though low level ripple can be achieved by the employment of large reservoir capacitors (over 10,000μF per rail), line and load regulations cannot be ensured.

To meet all the desired features the use of switched-mode power supplies consists in a feasible alternative. These topologies offer good regulation and permit a higher level of system integration, thus comprising a less costly and bulky solution. The ripple on the voltage rails is defined by the power supply output impedance, which is affected by the output filter of the converter and the closed loop control strategy [2]. It is clear that the choice of a control scheme over another can determine the overall system performance, so it becomes interesting to analyze the behavior of a switched-mode power supply topology for different closed loop controllers. In this paper, the influence of linear and nonlinear passivity-based control techniques on the power supply performance will be evaluated.

This paper is organized as follows: Section II presents a simple method to estimate the ripple magnitude on the voltage rails by means of the output impedance of the converter. Section III presents the used converter topology and its small-signal modelling. Section IV shows the compared control schemes. Section V presents the small-signal analysis for the compared control techniques and estimate the systems performance. Section VI shows the experimental results for the designed converter. The paper conclusions and discussions are presented in Section VII.

II. Output Ripple Estimation

The ripple seen on the voltage rails of a power supply used in audio amplification systems is generated by the interaction of the power supply output impedance with harmonic components inserted in the delivered current [3]. Such components appear due to the operation of the audio power amplifier, as discussed in [4]. Assuming that the reference audio signal has a sinusoidal profile and the voltage rails are regulated, the delivered current for a class AB linear amplifier would present a full-wave rectified sinus waveform, as shown in Fig. 1.

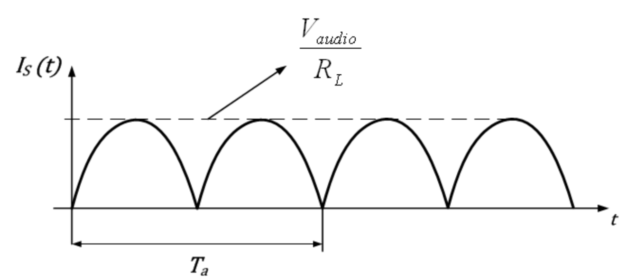

Fig. 1. Delivered current waveform.

Where:

V_{audio}	- Peak voltage of the amplified audio signal.
T_a	- Period of the audio signal.
R_L	- Amplifier output load (loudspeaker).

The amplitude of the harmonic components in the delivered current can be found by applying a Fourier Series on the waveform described in Fig. 1, which results in:

$$i_S(t) = \frac{V_{audio}}{R_L}\left[\frac{2}{\pi} - \frac{4}{\pi}\sum_n \frac{1}{n^2-1}cos(n\omega_a t)\right] \\ n = 2, 4, 6, 8... \tag{1}$$

Where:
- n - Harmonic order.
- ω_a - Audio reference angular frequency.

It becomes clear that the harmonic components inserted in the delivered current are even harmonics of the amplified audio signal. In order to prevent these components to cause voltage undulations on the voltage rails, the output impedance of the power supply should be sufficiently low. The relation between the amplitude of the ripple and the output impedance can be found by:

$$\Delta V_{CC} = I_{Sn} Z_{out} \tag{2}$$

Where:
- I_{Sn} - Amplitude of a n-order harmonic component.
- Z_{out} - Output impedance of the power supply.

Substituting I_{Sn} for the amplitude of the most significant component, *i.e.* the second harmonic, one could determine the magnitude of the normalized ripple as in:

$$k = \frac{4}{3\pi}\frac{V_{audio}}{V_{CC}}\frac{Z_{out}}{R_L} \tag{3}$$

Where:
- k - Normalized ripple amplitude.
- V_{CC} - Power supply output rail voltage.

The relation described in (3) can be used to estimate the magnitude of the ripple on the voltage rails by means of some amplified audio signal characteristics and the output impedance of the power supply. Such relation will be employed throughout this work to aid in the evaluation of the system performance.

III. Power Supply Topology

The power supply unit used in this work is based on a full-bridge switched converter, shown in Fig. 2.

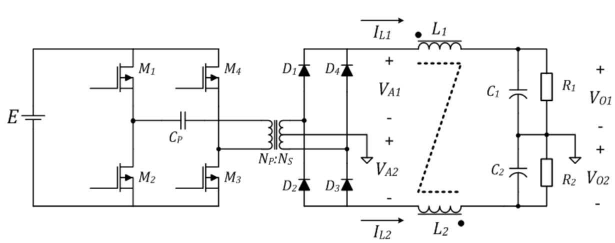

Fig. 2. Power stage structure of the audio power supply.

Some alterations in the conventional structure of the converter were made: the output stage was mirrored, so it could provide a dual voltage rail to power up a single-ended amplifier; the inductors of the output filters were coupled in the same magnetic core, in order to increase the symmetry between the voltage rails. The latter modification was necessary because the used converter allows only the control of the voltage between the both rails, *i.e.* the individual rails are not controlled. As each rail is exposed to different load profiles an unbalance on the output voltages is ought to happen. The coupled inductor minimizes this unbalance, enhancing the symmetry [4]. Table I shows the converter components and parameters used in this work.

TABLE I
Full bridge converter parameters.

Parameter	Symbol	Value
Switching Frequency	F_S	96kHz
Voltage rail	V_{O1}; V_{O2}	35V
Minimum input voltage	E	153V
Transformer turn ratio	$\frac{N_P}{N_S}$	0.72
Blocking capacitor	C_P	10μF
Output filter inductor	L_1;L_2	185μH
Output filter capacitors	C_1;C_2	66μF or 330μF
Equivalent output resistor	R_1;R_2	6.28Ω
Inductor magnetic coupling	k_{mag}	0.95

Since the control scheme could only regulate the voltage between the both output rails, it is interesting to describe the state equations of the converter in a way that it would be seen as an equivalent buck converter. In order to do so, consider the following state equations of the two output stages:

$$\begin{cases} uV_{A1} = L_1\frac{dI_{L1}}{dt} + V_{O1} + L_M\frac{dI_{L2}}{dt} \\ I_{L1} = C_1\frac{dV_{O1}}{dt} + \frac{V_{O1}}{R_1} \end{cases} \\ \begin{cases} uV_{A2} = L_2\frac{dI_{L2}}{dt} + V_{O2} + L_M\frac{dI_{L1}}{dt} \\ I_{L2} = C_2\frac{dV_{O2}}{dt} + \frac{V_{O2}}{R_2} \end{cases} \tag{4}$$

Where:
- L_M - Mutual inductance of the coupled inductors.
- μ - Switching command.

Assuming a variable change such as:

$$\begin{gathered} V_A = V_{A1} + V_{A2}; \\ V_O = V_{O1} + V_{O2}; \\ I_L = \frac{I_{L1}+I_{L2}}{2}; \\ L = L_1 = L_2 \\ C = C_1 = C_2 \\ R = R_1 = R_2 \end{gathered} \tag{5}$$

The equivalent buck converter state equations could be defined as:

$$\begin{cases} uV_A = 2(L+L_M)\frac{dI_L}{dt} + V_O \\ I_L = \frac{C}{2}\frac{dV_O}{dt} + \frac{V_O}{2R} + I_R \end{cases} \tag{6}$$

Where:
- I_R - Load perturbation and harmonic components

From the state equations found in (6) a set of transfer functions can be determined and so define a small-signal model for the switched converter. The most significant transfer functions are presented in (7) - (10) and the obtained model is shown as a block diagram in Fig. 3.

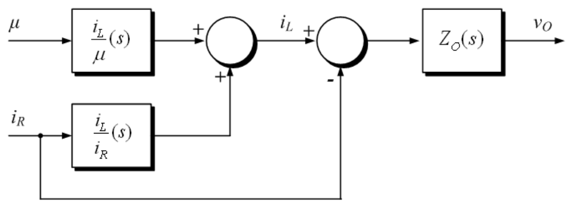

Fig. 3. Block diagram of the full bridge converter.

$$\frac{i_L}{\mu}(s) = \frac{V_A(RCs+1)}{RC2(L+L_M)s^2+2(L+L_M)s+2R} \quad (7)$$
$$\frac{i_L}{i_R}(s) = \frac{2R}{RC2(L+L_M)s^2+2(L+L_M)s+2R} \quad (8)$$
$$Z_O(s) = \frac{2R}{(RCs+1)} \quad (9)$$
$$v_O(s) = [i_L(s)-i_R(s)]Z_O(s) \quad (10)$$

The model shown in Fig. 3 presents an easy way to determine the influence of the load perturbation and harmonic components on the inductor current and the output voltage. The power supply output impedance can also be found by the output voltage response to the load perturbation.

IV. Compared Control Schemes

This work considered two different control techniques to be employed in the power supply unit: linear average control and passivity-based control. The first scheme is a conventional method used in several applications, which is based on the control of the average values of the converter states. The latter control strategy aims to control the dissipative structure of the converter by means of virtual damping insertion, thus providing asymptotic stability around a equilibrium point [7] and [8].

A. Linear controller

The block diagram of the linear control scheme used in this work is shown in Fig. 4.

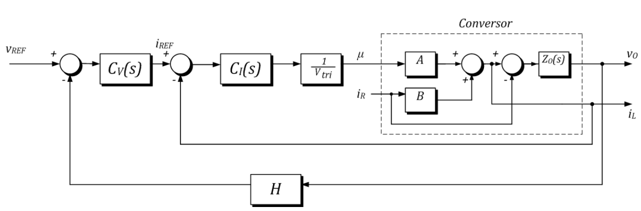

Fig. 4. Block diagram of the linear control scheme.

Where:

A	- $\frac{i_L}{\mu}$.
B	- $\frac{i_L}{i_R}$.
V_{tri}	- Triangular carrier amplitude. ($V_{tri} = 3V$)
H	- Voltage sensor gain. (H = 0.1)
$C_i(s)$	- Current compensator.
$C_V(s)$	- Voltage compensator.

It can be seen that the control circuit was divided in two compensation loops: an inner loop for current control and an outer loop for voltage regulation. It was chosen a Type II compensator topology for the linear controllers, as shown in Fig. 5. They were designed by an algorithm denominated *factor k approach*, discussed in [9]. Such algorithm describes a manner of defining the compensator parameters for a given phase margin and a crossover frequency.

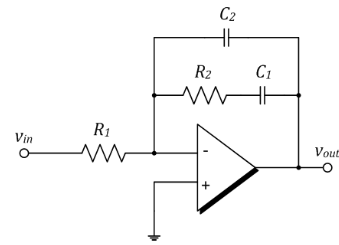

Fig. 5. Implemented circuit for a Type II linear compensator.

The compensator parameters used in this work are presented in Table II.

TABLE II
LINEAR CONTROLLER PARAMETERS.

Voltage Compensator		
Parameter	C = 66μF	C = 330μF
Phase Margin	60^o	
Crossover Frequency	3.8kHz	
R_1	10kΩ	10kΩ
R_2	8.2kΩ	39kΩ
C_1	15nF	2.2nF
C_2	1.8nF	560pF
Current Compensator		
Phase Margin	60^o	
Crossover Frequency	19.2kHz	
Parameter	C = 66μF	C = 330μF
R_1	10kΩ	10kΩ
R_2	22kΩ	22kΩ
C_1	1.2nF	1.2nF
C_2	100pF	100pF

B. Passivity-based controller

The passivity-based controller for a buck-like converter can be derived from the converter state equations as described in [6], [5] and [4]. The controller equations considered in this work are shown in (11).

$$\begin{cases} \dot{z_{d2}} = \frac{2}{C}(z_{d1} - \frac{1}{2R}z_{d2}) \\ \mu = \frac{1}{V_A}[2(L+L_M)\dot{z_{d1}} + z_{d2} - R_S(i_L - z_{d1})] \end{cases} \quad (11)$$

Where:

z_{d1}	- Inductor current reference.
z_{d2}	- Estimated output voltage.
R_S	- Series virtual damping parameter.

These equations determine an indirect control topology, *i.e.* the system controls the inductor current and the voltage is defined by the converter behavior. The assumed inductor current reference is shown in (12).

$$z_{d1} = \frac{1}{2R}V_{Od} + k_p(V_{Od} - v_O) + k_i \int_0^t [V_{Od} - v_O(\tau)]d\tau \quad (12)$$

Where:

- V_{Od} - Desired output voltage (70V).
- k_p - Proportional gain (k_p = 1).
- k_i - Integral gain, used to prevent steady state errors ($k_i = 100$).

The passivity-based controller was implemented by an analog circuit as the one shown in Fig. 6, the controller parameters are resumed in Table III.

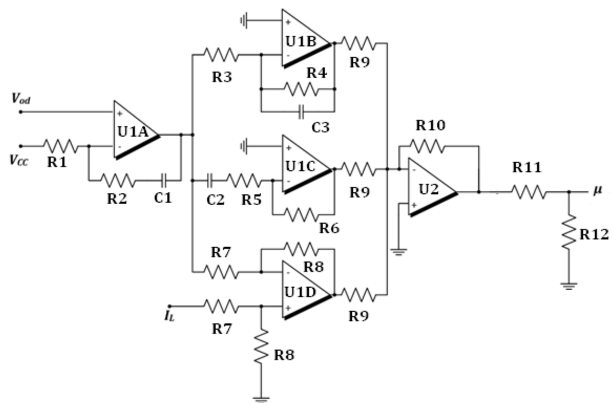

Fig. 6. Implemented passivity-based controller structure.

TABLE III
PASSIVITY-BASED CONTROLLER PARAMETERS.

Parameter	C = 66uF	C = 330uF
U_1, U_2	LM6171	
R_1	2.2kΩ	
R_2, R_8	22kΩ	
R_3, R_6, R_7, R_9	10kΩ	
R_4, R_{11}, R_{12}	12kΩ	
R_5	1.8kΩ	
R_{10}	4.7kΩ	
C_1	47nF	
C_2	5.6nF	
C_3	33nF	180nF

V. Closed-Loop System Behavior

In this section, the converter model described in Section III and the control schemes discussed in Section IV will be used to realize a small-signal analysis of the power supply performance. The main purpose was to evaluate the effect of the control schemes in the closed loop gain and the output impedance of the switched converter.

Through Fig. 7, the influence of the output capacitor variation can be perceived. For the passivity-based control, the increase of the capacitor value causes a reduction in the system bandwidth. At the linear control, this reduction is more subtle, but there is an increase in the loop gain overshoot near the cutoff frequency. In spite of that, it can be seen also that the passivity-based control presents a much wider bandwidth than the linear control system.

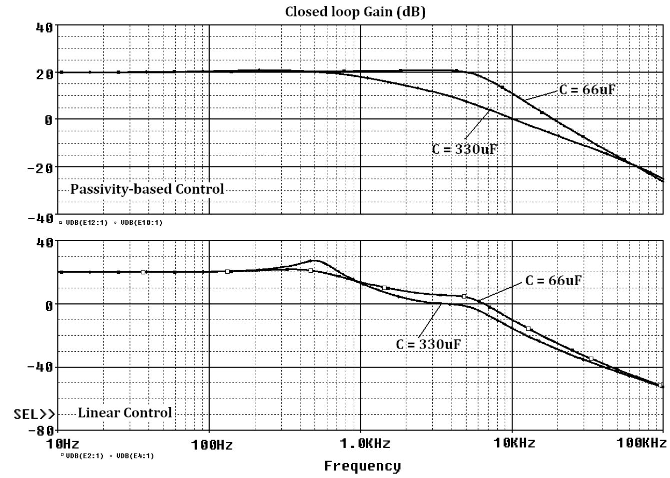

Fig. 7. Closed loop gain for linear and passivity-based controlled buck converters.

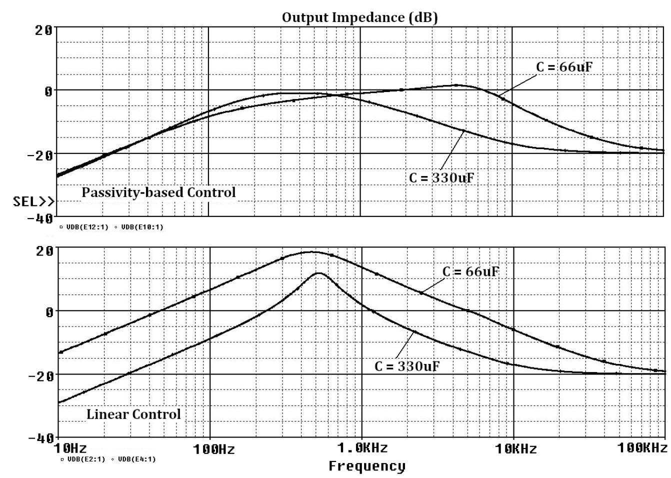

Fig. 8. Closed loop output impedance for buck converter.

The control scheme also interferes with the converter output impedance in a way shown in Fig. 8. Again the output capacitor influence can be noticed, for the linear control technique, the increase in the capacity provides an output impedance reduction of circa 45%. For the passivity-based control, the capacity variation causes the alteration of the output impedance form, decreasing it in the high frequency range and smoothly increasing it at the low frequency region. Comparing the obtained output impedance between the control schemes, it can be seen that independently of the output capacitor used the passivity-based control shows a smaller output impedance, which indicates that the resulted voltage rail ripple will be lower with this control topology.

Table IV presents some features towards the converter closed-loop behavior and performance, which can be derived from the loop gain and output impedance curves shown above.

TABLE IV
CONVERTER BEHAVIOR PARAMETERS.

Parameter	Passivity-based Control		Linear Control	
	C = 66μF	C = 330μF	C = 66μF	C = 330μF
Closed loop gain				
Bandwidth	6.6kHz	1.1kHz	730Hz	820Hz
Overshoot	0dB	0dB	1.7dB	7.4dB
Output impedance				
Maximum value	1.18Ω	0.90Ω	8.51Ω	3.89Ω
Frequency of maximum value	4.4kHz	400Hz	450Hz	520Hz

It is important to mention that the point of maximum output impedance will also be the point of maximum ripple magnitude on the voltage rail, but the audio signal frequency in which this maximum ripple occurs will be the half of the one shown in Table IV. Such different is explained by the relation between the reference audio frequency and the most significant harmonic component in the delivered current, which determines that the component responsible for causing the ripple is related to the second harmonic of the audio signal.

VI. EXPERIMENTAL RESULTS

A prototype of the designed full bridge converter was built to verify the theoretical observations. The experiments were conducted considering a class AB audio power amplifier as the power supply load, an amplified audio signal of $50V_{pp}$ and an amplifier load of 5Ω.

In order to verify the behavior of the ripple on the voltage rails over the audio-band, a frequency sweep of the audio reference signal was performed. The obtained results are summarized in Fig. 9, for the passivity-based control, and in Fig. 10, for the linear control.

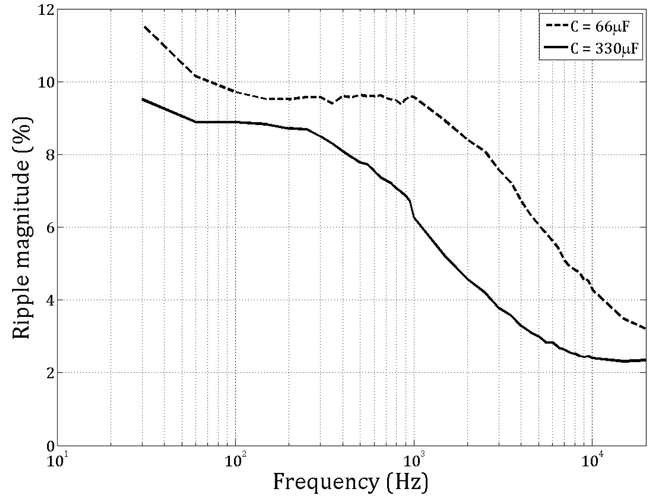

Fig. 9. Ripple magnitude behavior for a passivity-based control.

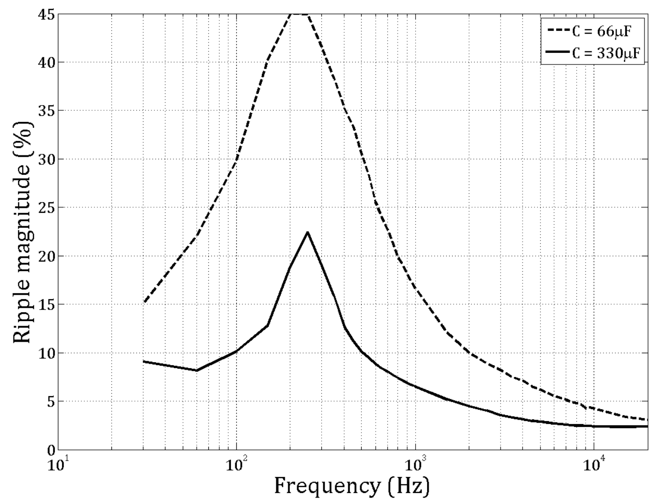

Fig. 10. Ripple magnitude for a linear control.

It can be seen that the output filter capacitor variation provides a reduction in the ripple magnitude for both control techniques, as expected from the theoretical analysis. The linear controlled system presents a ripple behavior that follows the output impedance shown in Fig. 8. Utilizing the relation described in (3) and the output impedances presented in Table IV the estimated ripple for a linear controlled system and output filter capacitor of 66μF was 48%, the experimental results shows a 45% ripple magnitude, which is close to the theoretical value. The same occurs for the 330μF capacitor were the theoretical ripple would be 22% and the actual one is 23%. The passivity-based controlled converter, however, has shown a different behavior, specially in the low frequency range. Such situation is caused by the load unbalance seen by each rail over the amplifier operation, as commented in Section III. The obtained ripple magnitudes are higher than the estimated by the theoretical model, but even so, compared to the linear system, the resulted performance with passivity-based controller is better.

Fig. 11 presents the comparison of the ripple waveforms on the positive voltage rail for both control schemes and both output filter capacitors at 250Hz, which represents the worst case for ripple magnitude in the linear controlled system as stated by Fig. 10. Such waveforms corroborate with the observations made so far towards the behavior of the two control techniques and the influence of the output filter capacitor variations over the ripple magnitude.

Fig. 12 and Fig. 13 presents the waveforms for the output voltages of the audio system for a 330μF output filter capacitor. It can be noticed that, even though the increase of the output capacity improves the power supply performance, it is not sufficient to prevent the linear controlled system to cause the amplified audio signal clamp, which worsens the resulted audio quality. In other hand, such clamping could not be observed in the passivity-based system.

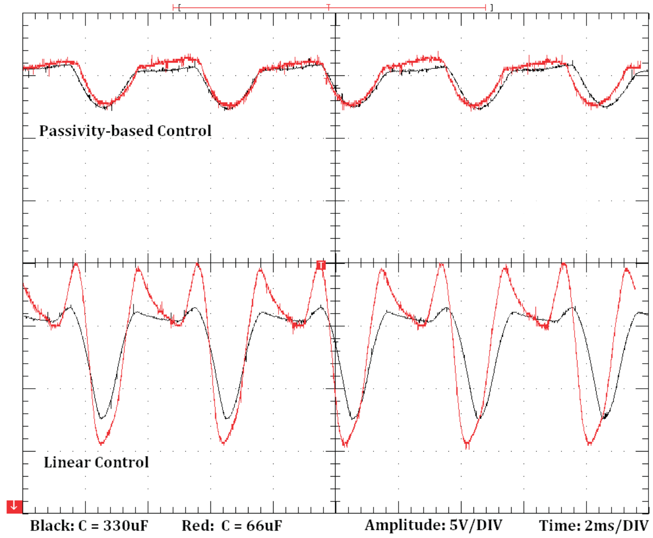

Fig. 11. Ripple waveforms for 250Hz audio signal.

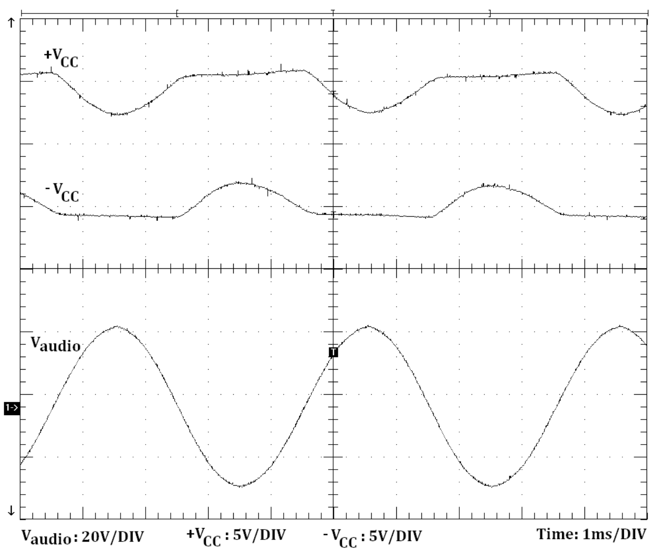

Fig. 12. Output voltages for passivity-based control at 250Hz.

VII. Conclusions

This work presented the comparison of the influence of linear and passivity-based control for switched-mode power supplies employed in audio amplification systems. The theoretical analysis has shown that the ripple magnitude can be estimated through the closed loop output impedance and the amplitude of harmonic components which are present in the delivered current. The theoretical and experimental analysis have shown that the passivity-based control provides a better performance than the linear control, presenting low level ripple even with lower output filter capacitors, allowing a suitable behavior for the power supply and a higher system integration, by means of employment of smaller components.

In spite of the good performance, the passivity-based control presented a higher ripple than expected through the theoretical model, such difference is related to the converter structure used in this work. It indicates that the power supply performance could be further improved by substituting the full-bridge topology for one converter that provides the possibility of controlling each rail voltage in an independent manner. Such alternative will be addressed in future works.

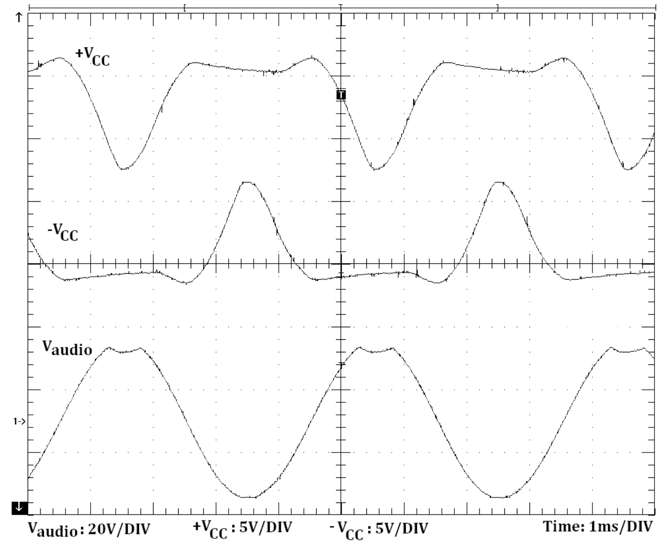

Fig. 13. Output voltages for linear control at 250Hz.

Acknowledgement

The authors would like to thank FAPEMIG for supporting and funding the research project.

References

[1] E. Mendenhall, *Power supply regulation in audio power amplifiers*, 113th Audio Engineering Society Convention, conference paper nº 5694, 2002.

[2] T. R. Oliveira; P. F. Donoso-Garcia, *Aplicação de Controle Baseado em Passividade a Fontes de Alimentação para Amplificadores de Potência*, Proceedings of the 9th Brazilian Audio Engineering Society Conference, São Paulo, Brazil, 2011.

[3] L. Risbo and T. Morch, *Performance of an All digital power amplification system*, 104th Audio Engineering Society Convention, 1998.

[4] T. R. Oliveira, *Estudo e implementação de uma fonte chaveada empregando controle baseado em passividade, para alimentação de amplificadores de potência de áudio,* Master Thesis, PPGEE-UFMG, 2011.

[5] E. A. Oliveira, *Aplicação do Controle Baseado Em Passividade Em Conversores Estáticos Operando Como Pré-reguladores de Fator de Potência,* Master Thesis, PPGEE-UFMG, 2008.

[6] E. A. Oliveira; *et al. Power Factor Correction via Passivity-Based Adaptive Controller Using a Buck Converter Operating in Continuous Mode,* IEEE Workshop on Control and Modeling for Power Electronics (COMPEL 08), p.p. 1–6, 2008.

[7] R. Ortega; A. Loría; P. J. Nicklasson; and H. Sira-Ramírez, *Passivity-based control of euler-lagrange systems: Mechanical, electrical and electromechanical applications,*, Springer–Verlag, 1^{st} edition, London, England, 1998.

[8] H. Sira-Ramírez and M. D. de Nieto , *A Lagrangian Approach to Average Modelling of Pulsewidth-Modulation Controlled Dc-to-DC Power Converters,*, IEEE transactions on Circuits and Systems - Fundamental Theory and Applications, vol. 43, nº 5, p.p. 427–430, 1996.

[9] W. H. Lei and T. K. Man , *A General Approach for Optimizing Dynamic Response for Buck Converter,*, AND8143/D - ON Semiconductor, Application Note, Rev.0, 2004.